Progress in Natural Science: Materials International 26 (2016) 467–476

HOSTED BY

Contents lists available at ScienceDirect

Progress in Natural Science: Materials International

journal homepage: www.elsevier.com/locate/pnsmi

Original Research

Optical absorption of $(Ag\text{-}Au)_{133}(SCH_3)_{52}$ bimetallic monolayer-protected clusters

Alessandro Fortunelli[a,*], Mauro Stener[b,*]

[a] CNR-ICCOM, Consiglio Nazionale delle Ricerche, via G. Moruzzi 1, I-56124 Pisa, Italy
[b] Dipartimento di Scienze Chimiche e Farmaceutiche, Università di Trieste, Trieste I-34127, Italy

ARTICLE INFO

Keywords:
Nanoalloys
Gold nanomolecules
Electronic excited states
Homotops
Transition electron density

ABSTRACT

The evolution of the optical absorption spectrum of bimetallic Ag-Au monolayer-protected clusters (MPC) obtained by progressively doping Ag into the experimentally known structure of $Au_{133}(SR)_{52}$ was predicted via rigorous time-dependent density-functional theory (TDDFT) calculations. In addition to monometallic $Au_{133}(SR)_{52}$ and $Ag_{133}(SR)_{52}$ species, 5 different $(Ag\text{-}Au)_{133}(SR)_{52}$ homotops were considered with varying Ag content and site positioning, and their electronic structure and optical response were analyzed in terms of Projected Density Of States (PDOS), the induced or transition electron density, and Transition Component Maps (TCM) at selected excitation energies. It was found that Ag doping led to the effects rather different from those encountered in bare metal clusters. And it was also observed that Ag doping could produce structured spectral features, especially in the 3–4 eV range but also in the optical region if Ag atoms were located in the sub-staple region, as rationalized by the accompanying electronic analysis. Additionally, Au doping into the staples of Ag-rich MPC also gave rise to a more homogeneous induced electron density. These findings show the great sensitivity of the electronic response of MPC nanoalloy systems to the exact location of the alloying sites.

1. Introduction

Monolayer-protected metal clusters (MPC) represent a class of compounds of great intrinsic fundamental interest and with very promising applications in a variety of applications such as sensing, optoelectronics and catalysis [1,2]. Among these, the phenomena connected with optical response stem out as the most ubiquitous due to the unique physics exhibited by potentially delocalized and very polarisable metal electrons confined in nanometer-scale systems and immersed in a strongly interacting environment [3]. Despite the great interest arisen and the considerable effort devoted to investigating the properties of MPC, several questions still remain to be addressed and/or fully clarified.

Among the present challenges, one is certainly connected with the optics of medium-sized MPC, such as thiolate-protected gold clusters with a number of Au atoms in the range of 100–200. This regime is intermediate between the smaller Au nanomolecules and the larger Au nanoparticles which start to closely resemble bulk-like nanocrystals. In this size range it is known that, unlike the extended metal systems exhibiting Plasmon Resonances (i.e., collective excitations of electron oscillating under an external electric field), real plasmonic features are not yet emerged, and indeed such features do not appear until ~300 Au atoms [4,5]. Nevertheless, these systems present a distinct optical spectrum, with an intermediate character which may be convenient in targeted applications, with significant absorption intensity more intense than in smaller systems and a not-too-large size able to fit specific biological or inorganic niches.

The basic concept usually employed to interpret the optical spectrum of such intermediate composite systems is that of an interplay and coupling between metal-core, mixed metal/sulfur-shell, and organic-residue-shell [6]. However, to implement this concept and fully exploit the main advantage of MPC (their atomically precise composition), the knowledge of atomistic structure is necessary. Unfortunately, while there are tens of X-ray solved MPC crystal structures [1,2], only a few concern the size régime beyond 100 Au atoms, with the *largest* compound fully characterized so far being the $Au_{133}(SPh\text{-}^tBu)_{52}$ system [7,8]. As will be shown in more detail below, the Au atoms in the Au_{107} core of $Au_{133}(SPh\text{-}^tBu)_{52}$ are organized into concentric icosahedral(Ih)-like shells, coated by 26 $Au(SPh\text{-}^tBu)_2$ units or "staples". It is worth noting that this Ih-like sequence of geometric shells is interesting also in that it has connections with the proposed model for the still unknown structure of $Au_{144}(SR)_{60}$ [9]. It is thus possible to consider

Peer review under responsibility of Chinese Materials Research Society.
* Corresponding authors.
E-mail addresses: alessandro.fortunelli@cnr.it (A. Fortunelli), stener@units.it (M. Stener).

http://dx.doi.org/10.1016/j.pnsc.2016.09.002
Received 31 July 2016; Accepted 16 August 2016
Available online 07 October 2016

variations of this basic structure and investigate whether it is possible, e.g., to enhance its optical response by chemical means. One possibility which has been theoretically investigated in detail only recently but whose principles are nevertheless reasonably well understood (although not experimentally exploited so far) is certainly to play with the organic residues e.g. by exploiting conjugation with properly matched electronic energy levels of the ligands to amplify the MPC response [10]. A second possibility in the field of metal clusters is that of alloying, i.e., to mix different elements into the metal frame, in such a way that synergic effects are generated. Alloying is in general recognized as an important tool to tune the properties of metal clusters [11] and specifically their optical properties [3]. If one keeps the same metal frame and simply varies how this is populated by different metal elements, one can generate a combinatorial number of isomers, named 'homotops' in the nanoalloy field [12], thus greatly enlarging the spectrum of mechanical, electronic, and chemical properties of metal clusters. Indeed, promising results come from experiment. For example, a pioneering work of Kumara et al. shows that $(Ag\text{-}Au)_{144}(SR)_{60}$ alloyed MPC exhibit a significant enhancement of absorption intensity in the 400–550 nm region of the spectrum [13], and a plasmonic character has been claimed also for $(Au\text{-}Cu)_{144}(SR)_{60}$ MPC [14,15], whereas in $(Ag\text{-}Au)_{130}(SR)_{50}$ MPC the absorbance features are not as prominent as in the undoped cluster [16].

The theoretical interpretation of these observations is still under debate. While the alloying effects on optical properties are reasonably well understood in the case of bare metal clusters [17], in the relatively simple case of the Ag-Au system of $(Ag\text{-}Au)_{144}(SR)_{60}$, two different rigorous time-dependent density-functional theory (TDDFT) studies led to different results [18,19], with not so large enhancements of optical absorption of the Ag-alloyed clusters. Clearly, the further investigations are in order.

In order to explore and further understand this problem we choose $Au_{133}(SR)_{52}$ as the largest Au MPC whose X-ray structure is available, avoiding the issues connected with uncertainties about structure. And the rigorous TDDFT simulations of the optical absorption spectrum of selected $(Ag\text{-}Au)_{133}(SR)_{52}$ homotops were performed. To speed up calculations, we replaced the pH^tBu with CH_3 residues. The simplification of $Au_{133}(SPh^tBu)_{52}$ into $Au_{133}(SCH_3)_{52}$ drastically reduces the computational effort and, as shown in the right panel of Figure S8 of Ref. [7], does not introduce dramatic changes to the optical spectrum, at least at the level of its general appearance, while allowing one to efficiently explore alloying effects on the optical properties of medium-sized monolayer-protected clusters.

What we find is a complex but interesting panorama, in which the precise location of doping species seems to play an important role in determining the final spectral features, as rationalized in terms of an analysis of the electronic structure and excitations of these systems.

In this article, the optical absorption properties of bimetallic Ag-Au monolayer-protected clusters are thus investigated. The details of the computational methods are given, the results and discussions presented, and the conclusions summarized.

2. Computational approach

The structure of the $Au_{133}(SCH_3)_{52}$ cluster is pictorially illustrated in Fig. 1 as taken from the previous work [7,8]. It is derived from a combination of X-ray data and theoretical simulations on $Au_{133}(SPh\text{-}^tBu)_{52}$ and $Au_{133}(SCH_3)_{52}$ as described in the original reference [7]. The Au atoms are fixed at the experimentally determined X-ray coordinates of $Au_{133}(SPh\text{-}^tBu)_{52}$ [7,8] while the S, C, H atoms are first relaxed via density-functional theory (DFT) simulations for $Au_{133}(SPh\text{-}^tBu)_{52}$, and then after freezing the coordinates of the S atoms, the methyl groups of $Au_{133}(SCH_3)_{52}$ are finally relaxed via DFT [7].

The Au core of $Au_{133}(SR)_{52}$ is organized into concentric shells of icosahedral(Ih)-like symmetry. As illustrated in Fig. 1 and described in more detail in Refs. [14,15], a central atom is first surrounded by an Ih shell of 12 neighbors, a second Mackay-Ih shell of 42 further neighbors, further enclosed by a Au_{52} shell which is derived from the 60-atom rhombicosidodecahedron in anti-Mackay stacking [20] lacking 8 atoms (4 sets of trimers of the rhombicosidodecahedron are merged into single atoms lying approximately at the center of the triangles), and finally by 26 $Au(SR)_2$ monomeric staples.

Starting from this geometry, we generate $(Ag\text{-}Au)_{133}(SCH_3)_{52}$ homotops by simply replacing Au with Ag atoms without relaxing atomic coordinates. This is justified by the fact that Ag and Au have very similar radii, which allows us to disentangle electronic from geometric effects. The $(Ag\text{-}Au)_{133}S_{52}$ cores of the $(Ag\text{-}Au)_{133}(SCH_3)_{52}$ homotops thus generated are shown in Fig. 2, where the Ag frame in selected cases for the convenience of the reader were also showed separately.

The photo absorption spectra have been calculated at the TDDFT level, with the complex polarizability algorithm, according to the theoretical method described in detail previously [21,22]. The photo absorption spectrum $\sigma(\omega)$ is calculated by computing at each value of the photon energy ω, the imaginary part of the isotropic dynamical polarizability $\alpha(\omega)$:

$$\sigma(\omega) = \frac{4\pi\omega}{c}\mathrm{Im}[\alpha(\omega)]. \quad (1)$$

The isotropic dynamical polarizability is calculated for complex frequency, i.e. $\omega = \omega_r + i\omega_i$, where the real part ω_r is the actual photon frequency (energy), and ω_i is the imaginary part which refers to a broadening of the discrete lines, and is interpreted as the excited state finite lifetime [23]. For the calculation of the spectrum, the isotropic part of the tensor is extracted from its trace: $\alpha(\omega) = \frac{1}{3}\sum_{i=1}^{3}\alpha_{ii}(\omega)$, where the index i runs on the three spatial components x, y and z. The kernel K of the TDDFT is the sum of the coulomb and the XC contributions, the latter being approximated according to the Adiabatic Local Density Approximation (ALDA) [24]. More precisely the TDDFT equations are represented in the space of the density fitting auxiliary basis functions, so that the induced density assumes the expression of a linear combination of the density fitting functions times the coefficients: $\rho_z^{(1)}(\omega, \vec{r}) = \sum_{\mu}^{K} f_\mu(\vec{r}) b_\mu(\omega)$, and the following non-homogeneous system of linear algebraic equations is obtained:

$$[\mathbf{S} - \mathbf{M}(\omega)]\mathbf{b} = \mathbf{d}. \quad (2)$$

In Eq. (2) **S** is the overlap matrix between fitting functions, **b** is the unknown vector with the expansion coefficients $b_\mu(\omega)$ of $\rho_z^{(1)}$, **M** and **d** are a frequency-dependent matrix and vector whose elements are given in Ref. [21]. In practice, Eq. (2) is solved for each value of the photon energy. The method is implemented in a local version of the ADF program. The LB94 [25] exchange-correlation (xc-) functional was employed to obtain the KS orbitals and eigenvalues from the KS equations, while the exchange-correlation kernel which is approximated at the ALDA level [24] in the TDDFT part, is calculated taking the derivative of the LDA xc-potential [26]. A basis set of Slater Type Orbitals (STO) included in the ADF database of Double Zeta (DZ) quality has been employed. The program allows a simple choice of a subset of the ADF STO fitting functions in order to save computer time when some fitting functions are not necessary for an accurate description of the photo absorption spectrum. Such a choice is based on preliminary test calculations on the simple diatomic molecules Au_2, Ag_2, CS and H_2 for Au, Ag, C, S and H respectively. The calculations have been performed at scalar relativistic level with Zero Order Relativistic Approximation (ZORA) [27].

3. Results and discussion

In the following we focus on the presentation and discussion of the chosen homotops and their absorption spectra, and the analysis of these spectra in terms of induced or transition density [28] and

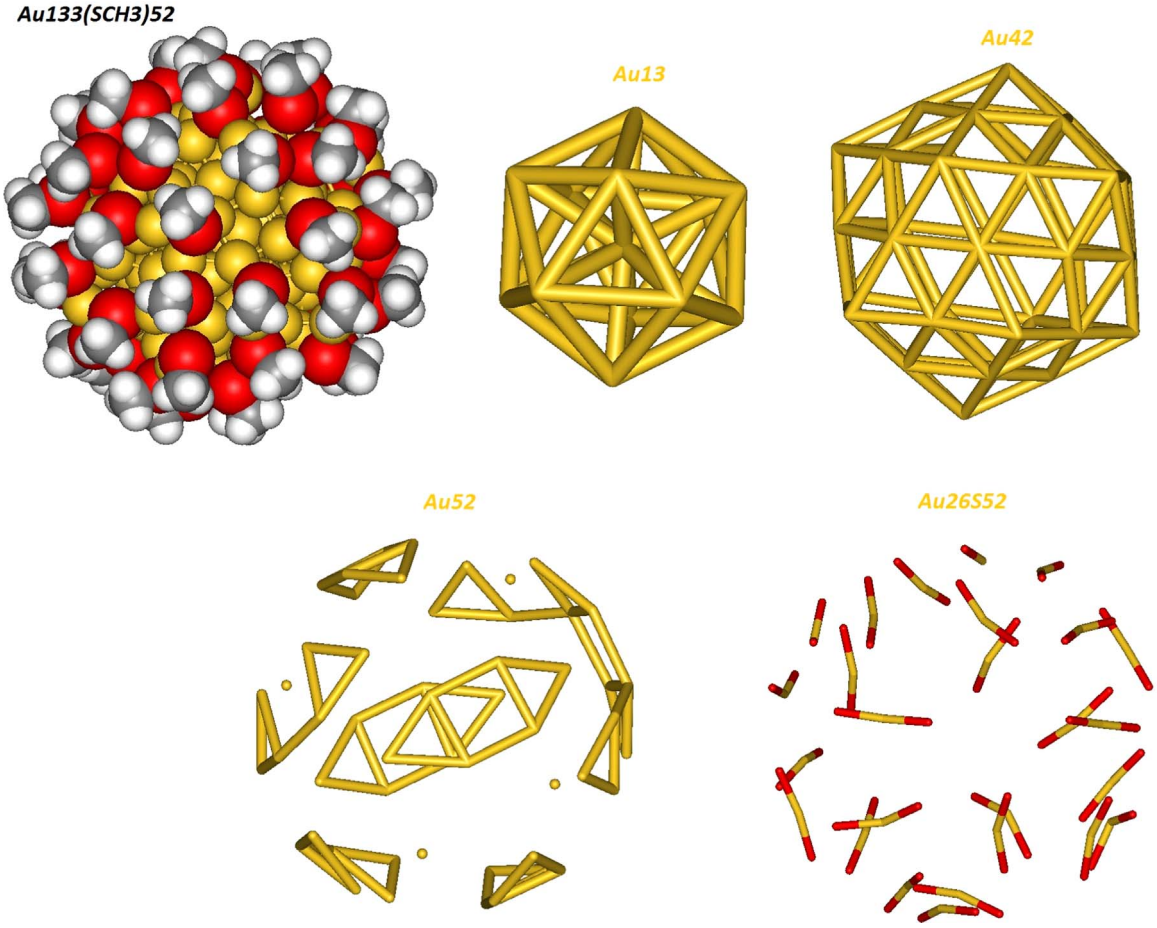

Fig. 1. Left-hand-top-most panel: Pictorial illustration of the structure of the $Au_{133}(SCH_3)_{52}$ cluster. Gold atoms as yellow spheres, sulfur in red, carbon in gray, and hydrogen in white. Other panels: the decomposition of the $(Ag\text{-}Au)_{133}S_{52}$ core into concentric quasi-Ih shells.

Projected Density Of States (PDOS).

The homotops considered here have been chosen by uniformly populating sites that are equivalent according to the quasi-Ih underlying symmetry of the metal frame, and are illustrated in Fig. 2 (with selected cases separately showing the Ag doping cluster for the convenience of the reader). In detail, $Au_{133}(SR)_{52}$, $Ag_{13}Au_{120}(SR)_{52}$, $Ag_{55}Au_{78}(SR)_{52}$, $Ag_{107}Au_{26}(SR)_{52}$, and $Ag_{133}(SR)_{52}$ correspond to a progressive alloying of the metal frame starting from the inner core (the Ih_{13} central cluster) to the further two shells (Ag_{55} and Ag_{107}) until the 26 Au atoms in the staples are also replaced with Ag in Ag_{133}. We thus expect that the properties (optical response) of these systems will follow a regular and progressive pattern. Additionally, $Ag_{26}Au_{107}(SR)_{52}$ and $Ag_{52}Au_{81}(SR)_{52}$ homotops have also been included, corresponding to the selective alloying of Ag into the staples (Ag_{26}) or in the outermost 52-atom shell of the metal core (Ag_{52}), respectively, to give the information on the effect of Ag doping into these sites variously interacting with the sulfur atoms of the ligands. This homotop selection strategy parallels that adopted in Ref. [18], allowing a direct comparison with the previous study.

Fig. 3 displays the absorption spectra of the alloyed MPC considered in this work. The spectra exhibit a non-trivial behavior as a function of Ag content, being much more complicated than that encountered in bare clusters [17] or even smaller MPC systems [29], thus, the current work demonstrates once more the opportunities provided by the unique and subtle interplay of metal-core, metal/sulfur-shell, and organic-residues in these composite systems [6]. Despite the complicated optical absorption behavior, some general features and trends are however discernible..

Starting from the un-doped $Au_{133}(SCH_3)_{52}$ cluster, it is first noted that the present LB94-predicted spectrum is qualitatively similar to that reported in Ref. [7] using the PBE [30] xc-functional, and also with the later calculations [31]. In this connection it is interesting to compare the absorption of bare and coated (MPC) clusters, e.g. Fig. 2 in Ref. [32] (in which the high-energy region suffers from limitations due to the number of extracted roots) or Fig. 3 of Ref. [33] with Fig. 3, S8 in Ref. [7] or the present calculations, although in the former case the LB94 xc-functional was employed in the TDDFT calculations, whereas in Ref. [7] the PBE xc-functional was employed. An analysis at the PBE level has been recently proposed [31], suggesting that in Au MPC one finds an enhancement of optical absorption, interpreted as a synergic effect between the electronic polarization of the Au metal core and the dielectric ligands. This contention however is not supported by earlier analyses [4,7,18,34] nor by the present results, from which the absorption intensity in the optical range of $Au_{144}(SR)_{60}$ and $Au_{\sim 144}$ bare clusters come out as comparable. As will be discussed in the following, the optical enhancement or depression in these medium-sized MPC (not connected with plasmonic phenomena which are absent at this size) is determined by an interplay of damping due to s/d mixing in bare clusters vs. coupling of metal and ligand orbitals in MPC. In this connection it is worth noting that in thiolate-protected Ag clusters large enough to exhibit a real (at least incipient) plasmon resonance coating usually produces a damping of the optical absorption [35].

It is necessary to analyze in more detail the main features and trends of the results presented in Fig. 3. Firstly, as noted in previous work [34] the absorption of these systems in the optical range (i.e., from 1.5 to 3 eV) corresponds to an unstructured monotonous increase – with the exception of $Ag_{52}Au_{81}(SR)_{52}$, that will be discussed below.

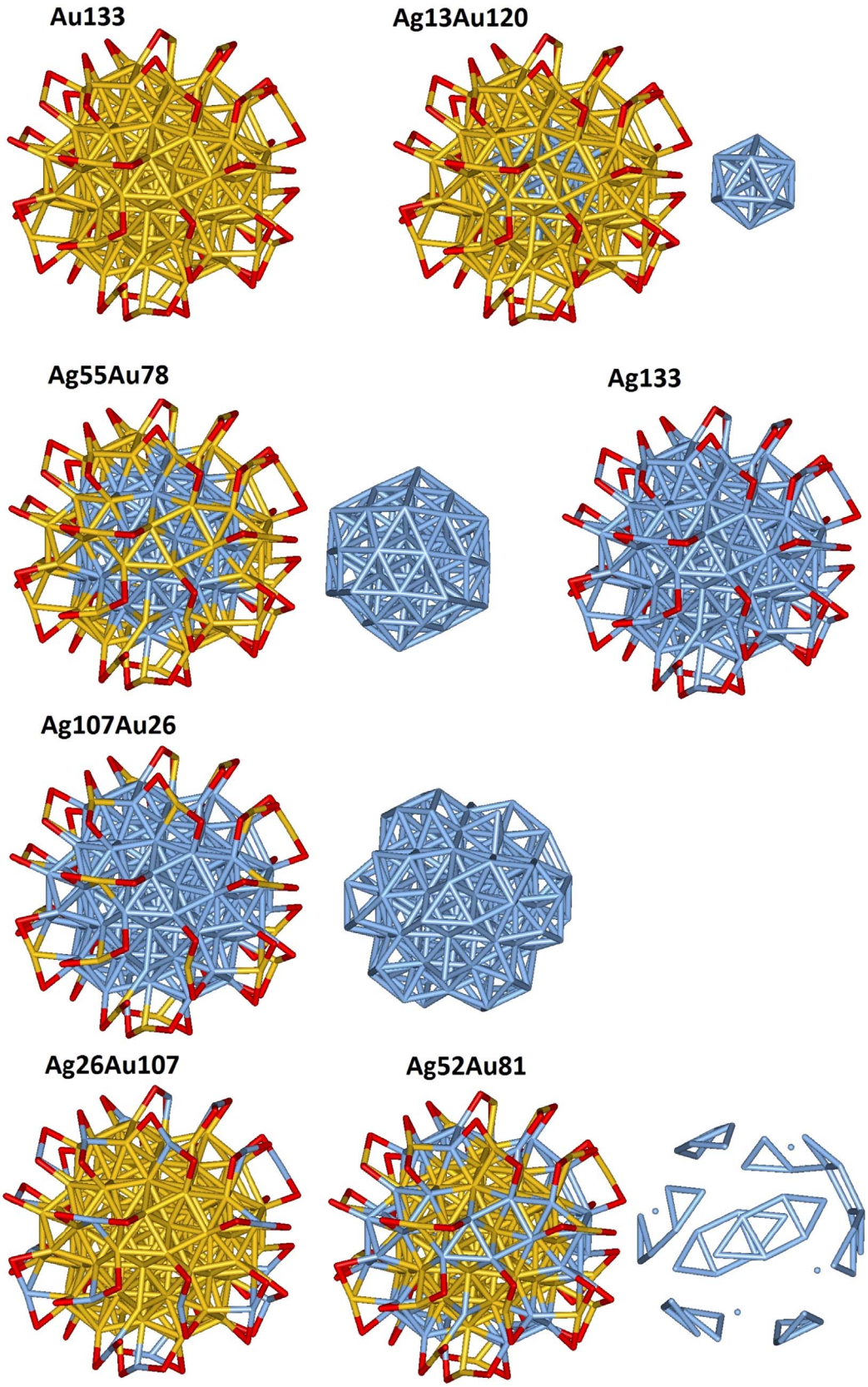

Fig. 2. Pictorial illustration of the $(Ag\text{-}Au)_{133}(SCH_3)_{52}$ homotops considered in this work. For convenience of the reader and clarity of illustration, CH_3 residues are omitted while the Ag doping cluster is explicitly shown next to the $(Ag\text{-}Au)_{133}S_{52}$ pictures in selected cases. Color coding as in Fig. 1.

The reason of this behavior is that the electronic excitations in this interval are essentially tails of major phenomena occurring at higher energies. In this context the presence of the coating shell of ligands has an ambivalent effect. On the one hand, it produces a charge compression (decrease of surface polarizability) and change transfer (decrease of the number of metal free electrons in favor of thiolate sulfur atoms).

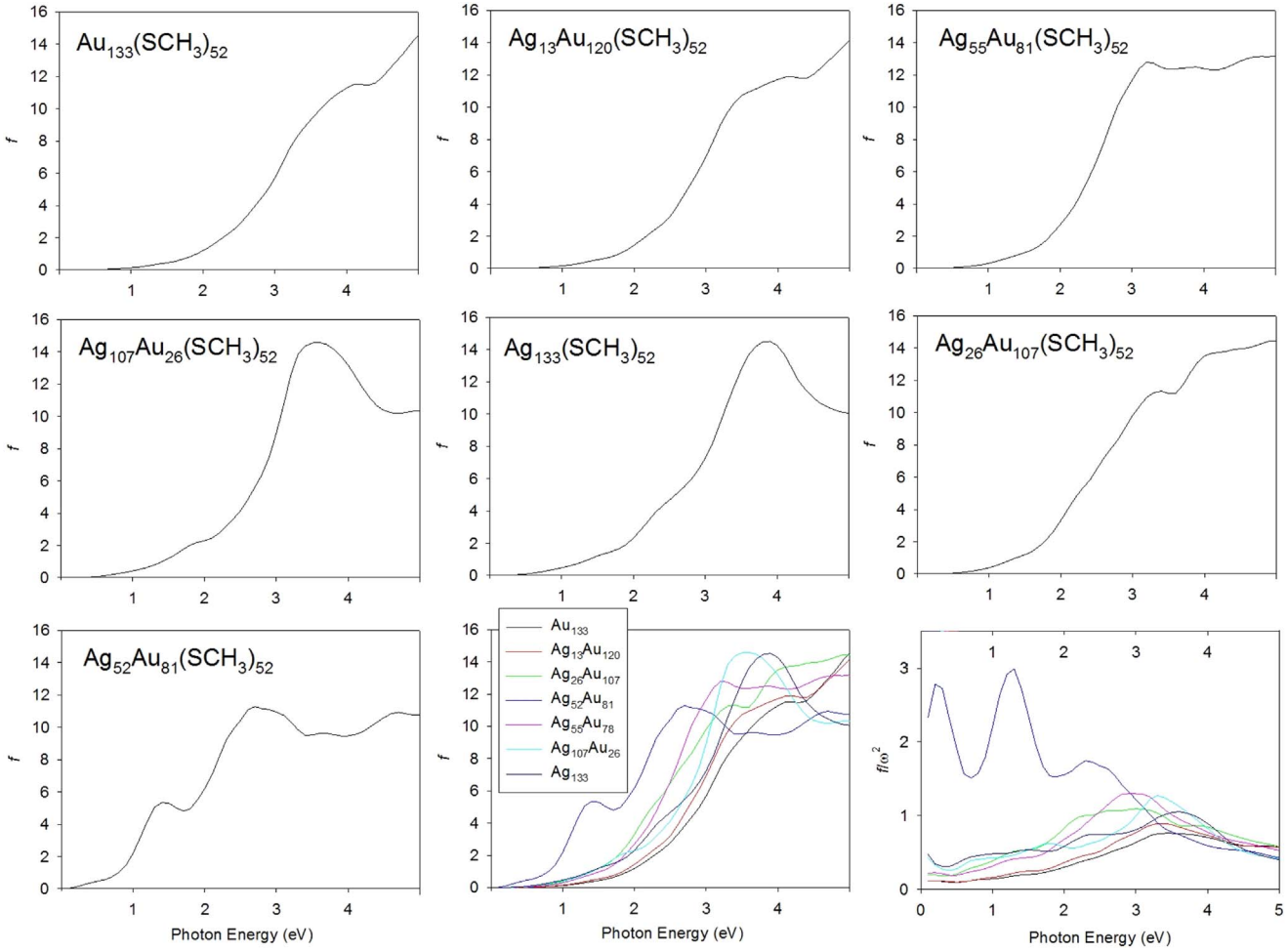

Fig. 3. The first 7 panels from top/left to bottom/right display TDDFT absorption spectra of the alloyed MPC considered in this work (each composition is explicitly indicated). f is the oscillator strength and is a-dimensional, while excitation energies (ω) are given in eV. The last 2 panels show a synoptic summary of all spectra and the same plots reported as f/ω^2 in the ordinate, respectively.

On the other hand, it allows orbital coupling with Au–S bonds, and thus decreases the damping due to s/d coupling in pure Au electronic states. Eventually, the oscillator strengths in the optical region have a moderate strength, not exceeding a value of roughly ≈8. Secondly, in the near-UV range, some structured features start to appear in the spectra, especially at higher Ag content. In particular, the shoulder between 3 and 4 eV already present in $Au_{133}(SR)_{52}$ becomes more and more pronounced with increasing Ag doping, until it turns into a clear maximum for $Ag_{107}Au_{26}(SR)_{52}$ and $Ag_{133}(SR)_{52}$.

The trend is however non-monotonous and in part counter-intuitive. Up to $Ag_{55}Au_{78}(SR)_{52}$, in fact, the absorption intensity shifts to the red (low-energy) region by increasing Ag content, whereas it shifts back to the blue (high-energy) region when $Ag_{107}Au_{26}(SR)_{52}$ and then $Ag_{133}(SR)_{52}$ are considered. This is at variance with the usual expectation from bare (Ag-Au) systems in which Ag doping always draws intensity to the blue and produces a significant increase in oscillator strength [17]. The rationale for the behavior here encountered is that – as will be discussed further below in conjunction with the analysis of transition density and PDOS – the optical absorption in these systems is not yet plasmonic, and is not associated with a standard surface plasmon resonance [4,5,34]. Therefore, at variance with bare metal clusters whose surface polarizability at their uncoated surfaces is typically enhanced by the introduction of Ag (and correspondingly the absorption intensities are much more intense), here the Ag introduced at the center of the cluster at low content does not take part to excitation phenomena and basically only produces a smaller HOMO-LUMO gap, hence drawing some intensity to the red, whereas only at high Ag composition does the absorption become dominated by the dopant element, with higher characteristic frequencies, thus shifting the absorption to the blue and creating a maximum in the near-UV.

In this scenario, selective doping into the staple metals atoms, $Ag_{26}Au_{107}(SR)_{52}$, does not stand out as qualitatively different. Nevertheless, one can observe a stronger red-shift due to a larger per-atom increase of inter-shell polarizability. This is a first hint that positioning of dopants in appropriate places of the metal frame can give rise to distinct effects as previously seen e.g. in Ag-Pt bare clusters [36]. Indeed, this is confirmed by selective doping into the sub-staple shell in $Ag_{52}Au_{81}(SR)_{52}$, leading to interesting irregularities.

$Ag_{52}Au_{81}(SR)_{52}$ in fact exhibits a strong shift of intensity into the optical region, with two well developed maxima at around 1.3 eV and 2.7 eV. We underline again that this is in stark contrast with bare and smaller MPC clusters [3], in which Ag doping usually leads to a blue shift of absorption peaks. The reason for this unexpected finding is that in $Ag_{52}Au_{81}(SR)_{52}$ Ag is doped at the interface between the metal core and the staple shell, thus simultaneously retaining most of its metal character but also interacting directly with the sulfur atoms of the ligands. In this situation, the energy of excitations between the metal-core and the metal/sulfur-shell is lowered, as shown by the PDOS and transition density analysis below, thus bringing about significant peaks in the optical region. A comparison with the $(Ag\text{-}Au)_{144}(SR)_{60}$ case [18,19] shows some similarity but also a stronger increase in intensity upon Ag doping into sub-staple sites in the $(Ag\text{-}Au)_{133}(SR)_{52}$ system, thus further demonstrating an interesting dependence of alloying

effects also on the underlying atomistic MPC structure. The emerging panorama is therefore rather complex.

It is underlined that a by-product of this analysis is the need of using reliable and accurate TDDFT approaches to properly investigate optical phenomena in medium-sized MPC. The pronounced sensitivity of the electronic response to the precise distribution of alloying elements makes that semi-classical or effective Hamiltonian or approximate approaches with their inherently averaged description of the ground, and the excited-state wave functions and potentials do not seem capable of capturing the subtle orbital coupling to determine the shift of intensity upon alloying across the 1–4 eV range. Also, the fact that the most interesting changes occur in the high-energy (near-UV) region of the spectrum makes that the approaches based on extracting a limited number of roots of the Casida matrix [18] may miss some enhancement effects, and thus the methods able to effectively cover the high-energy spectral regions such as those here employed [21,22] are absolutely required to investigate these phenomena.

It is often useful to introduce an alternative way of reporting absorption plots via the quantity f/ω^2, where f is the oscillator strength, which better highlights changes in intensity especially in cases such as the present ones in which variations over a monotonously increasing background are present. We then report this quantity for all the clusters here considered in the last panel of Fig. 3. Indeed, $Ag_{52}Au_{81}(SR)_{52}$ stands out more clearly from this plot with two well resolved peaks at 1.3 and 2.3 eV. It should be noted that a maximum in f/ω^2 also appears for this cluster at very low-energy (below 0.5 eV). However this is only an artifact due to a very small shoulder in absorption at low energy which is amplified by the ω^2 denominator. This is not physically significant and moreover, in the real system, it will be washed out by thermal effects here neglected.

An informative analysis of electronic excitations involves the induced or transition electron density $\rho_{tr}(\mathbf{r},\omega)$ as defined in equation 5.4.5 of Ref. [28]. This quantity corresponds to the variations or changes in electron density induced by the exciting field, with their positive or negative sign, and the plots of this induced or transition electron density are particularly useful to provide a visual representation of excitations. Fig. 4 reports the space plots of such a quantity for each cluster here considered, each plots are taken at a frequency ω approximately corresponding to the maximum in the quantity f/ω^2. We focus on the maxima in f/ω^2 quantity as they are more representative being less affected by the increasing background in absorption. However, we make an exception to this criterion for $Ag_{52}Au_{81}(SR)_{52}$, whose lowest-frequency maximum is an artifact as discussed above, hence the next maxima at around 1.3 and 2.3 eV have been considered. As noted above, these maxima lie in the far-VIS and near-UV region of the spectrum except for $Ag_{52}Au_{81}(SR)_{52}$, which is shifted to lower frequency in the optical region. We also note that only one orientation of the exciting electric field has been considered, but the optical anisotropy is modest for these rather symmetric structures. A nice trend is apparent from Fig. 4, which is in tune with general expectations. The induced density is initially fragmented in $Au_{133}(SR)_{52}$ into many, spatially confined, and rapidly alternating blobs, which progressively merge into larger and more homogeneous features going to $Ag_{13}Au_{120}(SR)_{52}$, $Ag_{55}Au_{78}(SR)_{52}$, and especially $Ag_{107}Au_{26}(SR)_{52}$, for which it acquires a classic dipolar appearance, somewhat perturbed by completing Ag doping into the staples in $Ag_{133}(SR)_{52}$. In passing, the fact that the dipolar character of the optical response of MPC at this size is more evident in $Ag_{107}Au_{26}(SR)_{52}$ than in $Ag_{133}(SR)_{52}$, which incidentally suggests that Au doping into the staples of pure Ag clusters might be beneficial for obtaining a more homogeneous optical response. The induced density also singles out which parts of the cluster are mostly involved in the electronic excitation, i.e., from which part density is moved into which part. In this connection for example it is interesting to observe that $Au_{133}(SR)_{52}$ and $Ag_{26}Au_{107}(SR)_{52}$ exhibit a visually immediately apparent similarity in their transition response, with only a larger involvement of the metal atoms of the staples in $Ag_{26}Au_{107}(SR)_{52}$, therefore justifying its enhanced adsorption intensity. Analogously, a comparison of the induced density of $Ag_{52}Au_{81}(SR)_{52}$ with that of $Au_{133}(SR)_{52}$ and $Ag_{55}Au_{78}(SR)_{52}$ shows a qualitative similarity especially with $Ag_{55}Au_{78}(SR)_{52}$, as well as a more homogeneous involvement of the whole cluster interface when the sub-staple shell is doped with Ag, in tune with the observed lowering of the frequency (energy) of this excitation mode.

To provide the information on the electronic structure of the clusters under study be useful to understand their optical response, it is customary to consider the plots of partial DOS as reported in Fig. 5. The partial DOS have been produced partitioning the total DOS with respect to the Mulliken population of S atoms and of the separate sp and d contributions of both Ag and Au atoms. It is useful to start with S-type contributions, which remains almost constant along the series. The only differences are apparent in $Ag_{26}Au_{107}(SR)_{52}$ and $Ag_{133}(SR)_{52}$, where the S partial DOS maximum around −11 eV looks more intense and sharper. It is worth noting that these are the only two systems which have the Ag atoms in the staple fragments. The maximum at −11 eV in S partial DOS is connected with the bonding interaction between S and the metal, while the contribution above the Fermi level (which lies at −10.1 eV for all clusters except for $Ag_{133}(SR)_{52}$ for which it lies at −10.3 eV) represents the anti-bonding counterpart which is enhanced when the bonding nature is more covalent, while for a pure ionic bond (M^+ SR^-) the S manifold would be totally occupied. With this picture in mind we can interpret the behavior of the S-atom partial DOS as an indication that when the Ag atoms are in the staples the Ag–S bond is less covalent (more ionic) than when the Au atoms are in the staples. It is convenient to compare the two pure clusters $Au_{133}(SR)_{52}$ and $Ag_{133}(SR)_{52}$: the sp bands are quite similar, there is a maximum between −12 and −11 eV, which represents the metallic counterpart of the M–S bond, followed by a secondary maximum just below the Fermi level, followed by an increase above the Fermi level, which is modulated giving three more features within the energy considered. The modulation is much more evident in $Ag_{133}(SR)_{52}$ than in $Au_{133}(SR)_{52}$. If we consider the metal d contribution for the pure clusters, it is not surprising to find a major role of the d band for gold: this is due to the relativistic effects which narrow the 5d-6s gap of gold with respect to the 4d-5s one of silver. The consequence is a more important contribution of the Au 5d also in the Au–S bond (around −11 eV), enhancing the covalent as well as directional nature of the bond. The mixed clusters represent intermediate situations: from $Au_{133}(SR)_{52}$ to $Ag_{55}Au_{78}(SR)_{52}$ a regular decrease of the Au(sp) and Au(d) contributions is apparent. However the partial DOS profile are all qualitatively very similar to $Au_{133}(SR)_{52}$, suggesting that the properties are governed mainly by gold electronic structure. On the contrary, with $Ag_{107}Au_{26}(SR)_{52}$ the silver partial DOS become the leading ones, so now the cluster electronic structure is governed by silver, gold partial profiles being reduced to a marginal role, with the exception of the Au(d) which remains comparable to the Ag(d).

The last tool we use in our analysis is plotting Transition Component Maps (TCM) as defined in Ref. [4] calculated at the photon energy corresponding to the absorption maxima and reported in Fig. S1. In this case of non plasmonic optical response, these plots are less informative than in the case of real plasmonic systems. Nevertheless, a most notable result from the plots of Fig. S1 is that all the contributions lie on the straight line which corresponds to the energy difference between virtual and occupied orbitals and equals the excitation energy. This confirms that there is no real coupling among one-electron excited configurations, ruling out any real plasmonic behavior [33]. In other words, in agreement with previous studies we find that MPC at this size do not exhibit any real plasmonic (collective) character, whose characteristic feature is an excited state(s) made up of a combination of very many single-electron modes. In more detail, for $Au_{133}(SR)_{52}$ and $Ag_{13}Au_{120}(SR)_{52}$ the two spots around −13 eV correspond to inter-band transitions from the Au(d) band to the Au(sp), the next two spots around −11 eV correspond to the transition from the S band to the

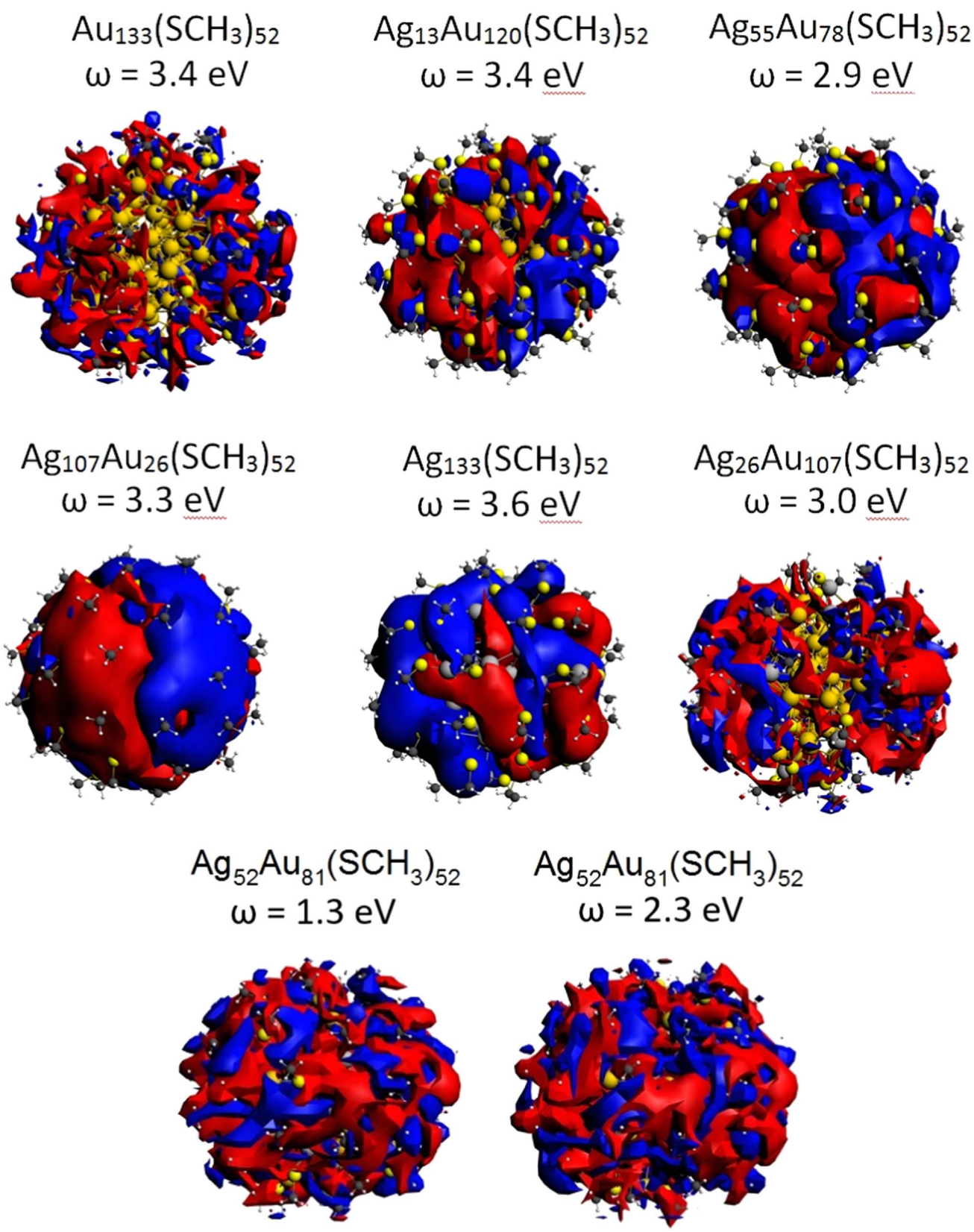

Fig. 4. Isocontour plots of transition or induced electron density corresponding to excitations with a frequency (explicitly indicated) centered at the maximum of f/ω^2 for each cluster as discussed in the text and with the exciting electric field oriented from left to right of the figures. The values of the isocontours are 0.05 e/Å^3 for $Au_{133}(SR)_{52}$, $Ag_{26}Au_{107}(SR)_{52}$ and $Ag_{52}Au_{81}(SR)_{52,}$ 10 e/Å^3 for $Ag_{13}Au_{120}(SR)_{52}$, , $Ag_{55}Au_{78}(SR)_{52}$, and $Ag_{107}Au_{26}(SR)_{52}$, and 50 e/Å^3 for $Ag_{133}(SR)_{52}$. Blue and red colors correspond to contours of opposite sign.

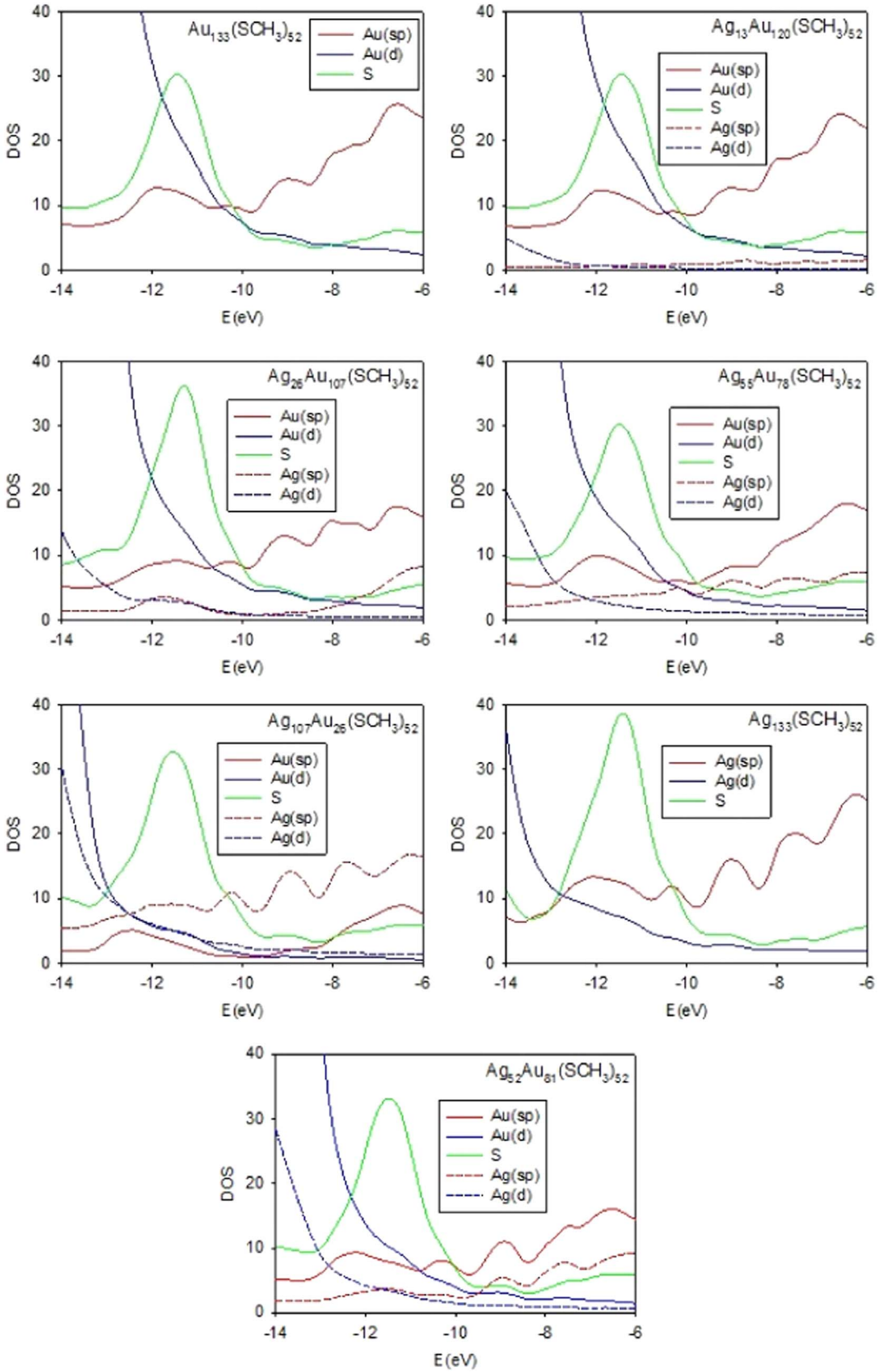

Fig. 5. Projected Density Of States (PDOS), obtained partitioning total DOS by Mulliken population of S atom, Au(sp), Au(d), Ag(sp) and Ag(d) contributions. The Fermi energy is −10.1 eV fpr all the clusters, except for $Ag_{133}(SR)_{52}$ for which it reads −10.3 eV.

Au(sp) band, then the next contribution at −10 eV is related to the intraband Au(sp) → Au(sp) transition. Considering that the partial DOS shapes remain almost constant along the cluster series, we can consider the variation of the TCM in the next terms. In $Ag_{26}Au_{107}(SR)_{52}$ and $Ag_{55}Au_{78}(SR)_{52}$, there is apparently a reduction of the role of the band at −13 eV (interband Au(d)→Au(sp)) as well as the band at −10 eV (intraband Au(sp)→Au(sp)), so the S→Au(sp) excitations are gaining more importance in these clusters. Moreover, for the $Ag_{107}Au_{26}(SR)_{52}$ and $Ag_{133}(SR)_{52}$ clusters, the effect is even stronger, so the S→Au(sp) excitations become the leading ones. Finally, the absorption of $Ag_{52}Au_{81}(SR)_{52}$ is outside the observed trend. As noted above, its absorption spectrum is in fact characterized by two features at 1.3 eV and 2.7 eV, while looking at the f/ω^2 quantity such features lie at 1.3 eV and 2.3 eV, and a spurious maximum is found just above zero energy. The feature at 1.3 eV corresponds to a pure Au(sp)→Au(sp) intraband excitation, while that at 2.3 eV corresponds to a mixing between the Au(sp)→Au(sp) intraband and the Au–S→Au(sp) interband excitations. Interestingly, the TCM at 2.3 eV of $Ag_{52}Au_{81}(SR)_{52}$ displays (although very weakly) some coupling with excited configurations with lower energy and intraband Au(sp) nature, that is a clear indication of an incipient plasmonic behavior.

So far we have focused exclusively on optical response, which is the topic of the present work. Before concluding, a few remarks on energetics are however in order. To thus aim, we introduce the definition of mixing energy for MPC compounds, which is commonly used in the field of nanoalloys. The mixing energy as a function of composition for a mixed A-B cluster can be defined as follows [37–39]:

$$\Delta[N_A, N_B]=E_{alloy}[N_A, N_B] - N_A E_A[N]/N - N_B E_B[N]/N \quad (3)$$

where $E_{alloy}[N_A, N_B]$ is the energy of a nanoalloy cluster composed of N_A atoms of the species A and N_B atoms of the species B, $N=N_A+N_B$ is the total number of atoms in the cluster, E_A [N] is the energy of a pure cluster of N atoms and E_B [N] is the corresponding quantity for the B species. The mixing energy $\Delta[N_A, N_B]$ is useful to compare the stability of nanoalloys of a given size, but a different chemical composition, since it provides a measure of how thermodynamically favorable is alloying at the given size and composition. In Fig. S2 of the SI we report such a quantity for the mixed clusters here considered by using the BP86 xc-functional [40]. We use the BP86 xc-functional instead of the LB94 xc-functional for these calculations because LB94 provides long-range Coulombic corrections to the potential and not the energy, while BP86 is a GGA xc-functional, which usually gives reasonably accurate energies for Au-containing compounds [41].

Clearly the positive values of mixing energies are connected with the fact that we do not relax the corresponding geometries. Nevertheless, these values suggest that $Ag_{13}Au_{120}(SR)_{52}$ and $Ag_{107}Au_{26}(SR)_{52}$ are the species with a higher stability, whereas the others seem roughly similar, although a slightly larger instability might be associated with $Ag_{52}Au_{81}(SR)_{52}$.

4. Conclusions

A first-principles time-dependent density-functional theory (TDDFT) investigation of the optical absorption spectrum for bimetallic Ag-Au monolayer-protected clusters (MPC) with formulae $(Ag-Au)_{133}(SCH_3)_{52}$ has been conducted. The experimentally known structure of $Au_{133}(SPh\text{-}^tBu)_{52}$ [7,8] is used as a framework in which Ag and Au atoms are positioned (thus allowing us to disentangle structural and electronic effects) and 5 different alloyed compositions in an interval between pure Au and Ag compounds are so sampled.

It has been found that Ag doping into middle-sized Au MPC is a different and more complex phenomenon with respect to that encountered in bare metal clusters. In this size range in which true plasmonic resonances are not yet developed and electronic excited states exhibit a predominantly single-particle character, the replacement of Au with Ag affects the optical spectrum with a strong dependence on the precise location of the Ag atoms in the homotops. The largest influence and enhancement in the optical region is associated with Ag-doping into the sub-staple sites, i.e. those in contact with the ligand sulfur atoms and at the interface between the metal core and the metal/ligand mixed shell. This is due to a drift of absorption intensity from the UV into the visible region associated with subtle changes in the alignment of energy levels of the metal-core/metal-sulfur-shell/organic-residue composite system, as rationalized on the basis of an analysis of the density of states (PDOS) and induced electron density. Additionally, in the opposite range of compositions, doping Au into the staple metal atoms of Ag-rich clusters seems to render the optical response more homogeneous (dipolar).

A by-product of the present analysis is that reliable and accurate TDDFT approaches are needed to properly investigate optical phenomena in medium-sized MPC, because their great sensitivity to the precise distribution of alloying elements undermines the accuracy of methods based on an averaged description of the electronic structure, while the fact that important changes are localized in the high-energy region of the spectrum requires approaches capable of describing correctly high-frequency electron oscillations.

Energetically, the mixing energy for MPC alloying (here defined for the first time) suggests that the most effective sites to promote optical absorption may not correspond to the energetically most favorable positions, and that meta-stable homotops with rather different optical properties depending on the synthetic procedure and experimental conditions may be populated, which seems to be in tune with the experimentally observed spread of optical data [13,14,16].

Acknowledgements

We thank Amala Dass for stimulating discussions and Luca Sementa and Giovanni Barcaro for providing the coordinates of the $Au_{133}(SCH_3)_{52}$ cluster. Computational research was performed in part using PNNL Institutional Computing at Pacific Northwest National Laboratory. Support from CINECA supercomputing centre within the ISCRA programme is also gratefully acknowledged.

Appendix A. Supplementary material

Supplementary data associated with this article can be found in the online version at doi: http://dx.doi.org/10.1016/j.pnsc.2016.09.002.

References

[1] H. Qian, M. Zhu, Z. Wu, R. Jin, Acc. Chem. Res. 45 (2012) 1470–1479.
[2] Tatsuya Tsukuda, Hannu Hakkinen (Eds.), Protected Metal Clusters: From Fundamentals to Applications1st ed., Elsevier, 2015 (ISBN 9780081000861).
[3] G. Barcaro, L. Sementa, A. Fortunelli, M. Stener, Phys. Chem. Chem. Phys. 17 (2015) 27952.
[4] S. Malola, L. Lehtovaara, J. Enkovaara, H. Häkkinen, ACS Nano 7 (2013) 10263–10270.
[5] Y. Negishi, T. Nakazaki, S. Malola, S. Takano, Y. Niihori, W. Kurashige, S. Yamazoe, T. Tsukuda, H. Häkkinen, J. Am. Chem. Soc. 137 (2015) 1206–1212.
[6] M. Zhu, C.M. Aikens, F.J. Hollander, G.C. Schatz, R. Jin, J. Am. Chem. Soc. 130 (2008) 5883.
[7] A. Dass, S. Theivendran, P.R. Nimmala, C. Kumara, V.R. Jupally, A. Fortunelli, L. Sementa, G. Barcaro, X. Zuo, B.C. Noll, J. Am. Chem. Soc. 137 (2015) 4610–4613.
[8] C. Zeng, Y. Chen, K. Kirschbaum, K. Appavoo, M.Y. Sfeir, R. Jin, Sci. Adv. 1 (2015).
[9] O. Lopez-Acevedo, J. Akola, R.L. Whetten, H. Grönbeck, H. Häkkinen, J. Phys. Chem. C 113 (2009) 5035–5038.
[10] L. Sementa, G. Barcaro, A. Dass, M. Stener, A. Fortunelli, Chem. Commun. 51 (2015) 7935.
[11] G. Barcaro, A. Caro, A. Fortunelli, Alloys on the nanoscale, in: R. Vajtai (Ed.) Springer Handbook: Nanomaterials, Springer, Berlin, 2013.
[12] J. Jellinek, E.B. E. B. Krissinel, Chem. Phys. Lett. 258 (1996) 283–292.
[13] C. Kumara, A. Dass, Nanoscale 3 (2011) 3064–3067.
[14] A.C. Dharmaratne, A. Dass, Chem. Commun. 50 (2014) 1722–1724.
[15] S. Malola, M.J. Hartmann, H. Häkkinen, J. Phys. Chem. Lett. 6 (2015) 515–520.
[16] V.R. Jupally, A. Dass, Phys. Chem. Chem. Phys. 16 (2014) 10473–10479.
[17] G. Barcaro, M. Broyer, N. Durante, A. Fortunelli, M. Stener, J. Phys. Chem. C 115 (2011) 24085–24091.

[18] G. Barcaro, L. Sementa, A. Fortunelli, M. Stener, Nanoscale 7 (2015) 8166–8167.
[19] S. Malola, L. Lehtovaara, H. Hakkinen, J. Phys. Chem. C 118 (2014) 20002–20008.
[20] E.G. Mednikov, M.C. Jewell, L.F. Dahl, J. Am. Chem. Soc. 129 (2007) 11619.
[21] O. Baseggio, G. Fronzoni, M. Stener, J. Chem. Phys. 143 (2015) 024106.
[22] O. Baseggio, M. De Vetta, G. Fronzoni, M. Stener, A. Fortunelli, Int. J. Quantum Chem. 116 (2016) 1603. http://dx.doi.org/10.1002/qua.25175.
[23] L. Jensen, J. Autschbach, G.C. Schatz, J. Chem. Phys. 122 (2005) 224115.
[24] E.K.U. Gross, W. Kohn, Adv. Quantum Chem. 21 (1990) 255.
[25] R. Van Leeuwen, E.J. Baerends, Phys. Rev. A 49 (1994) 2421.
[26] S.H. Vosko, L. Wilk, M. Nusair, Can. J. Phys. 58 (1980) 1200.
[27] E. van Lenthe, E.J. Baerends, J.G. Snijders, J. Chem. Phys. 99 (1993) 4597.
[28] R. McWeeny, Methods of Molecular Quantum Mechanics, 2nd ed., Academic Press, London, 1989.
[29] C. Kumara, C.M. Aikens, A. Dass, J. Phys. Chem. Lett. 5 (2014) 461–466.
[30] J.P. Perdew, K. Burke, M. Ernzerhof, Phys. Rev. Lett. 77 (1996) 3865–3868.
[31] K. Iida, M. Noda, K. Nobusada, J. Phys. Chem. C 120 (2016) 2753–2759.
[32] N. Durante, A. Fortunelli, M. Broyer, M. Stener, J. Phys. Chem. C 115 (2011) 6277–6282.
[33] O. Baseggio, M. De Vetta, G. Fronzoni, M. Stener, L. Sementa, A. Fortunelli, A. Calzolari, J. Phys. Chem. C 120 (23) (2016) 12773–12782.
[34] H.-Ch Weissker, O. Lopez-Acevedo, R.L. Whetten, X. López-Lozano, J. Phys. Chem. C 119 (2015) 11250.
[35] G. Barcaro, L. Sementa, A. Fortunelli, M. Stener, J. Phys. Chem. C 118 (2014) 12450–12458.
[36] G. Barcaro, L. Sementa, A. Fortunelli, M. Stener, J. Phys. Chem. C 118 (2014) 28101–28108.
[37] A. Fortunelli, A.M. Velasco, J. Mol. Struct. (Theochem) 487 (1999) 251–266.
[38] R. Ferrando, A. Fortunelli, G. Rossi, Phys. Rev. B 72 (2005) 085449.
[39] G. Barcaro, L. Sementa, A. Fortunelli, Phys. Chem. Chem. Phys. 16 (2014) 24256–24265.
[40] (a) A.D. Becke, Phys. Rev. A 38 (1988) 3098;
(b) J.P. Perdew, Phys. Rev. B 33 (1986) 8822.
[41] O.D. Häberlen, S.-C. Chung, M. Stener, N. Rösch, J. Chem. Phys. 106 (1997) 5189.